



Measurement report: Atmospheric new particle formation in a peri-urban site in Lille, Northern France

Suzanne Crumeyrolle¹, Jenni SS Kontkanen^{2,3}, Clémence Rose⁴, Alejandra Velasquez Garcia^{1,5}, Eric Bourrienne¹, Maxime Catalfamo¹, Véronique Riffault⁵, Emmanuel Tison⁵, Joel Ferreira de Brito⁵, Nicolas Visez⁶, Nicolas Ferlay¹, Frédérique Auriol¹, Isabelle Chiapello¹

¹ Univ. Lille, CNRS, UMR 8518 Laboratoire d'Optique Atmosphérique (LOA), 59000 Lille, France

² CSC - IT Center for Science, Espoo, Finland

³ Institute for Atmospheric and Earth system Research, University of Helsinki, Helsinki, Finland

⁴ Laboratoire de Météorologie Physique, LaMP-UMR 6016, CNRS, Université Clermont Auvergne, 63178, Aubière, France

⁵ IMT Nord Europe, Institut Mines-Télécom, Univ. Lille, Centre for Energy and Environment, F-59000 Lille, France

⁶ Univ. Lille, CNRS, UMR 8516 - LASIRE - Laboratoire de Spectroscopie pour les Interactions, la Réactivité et l'Environnement, F-59000 Lille, France.

Correspondence to: Suzanne Crumeyrolle (suzanne.crumeyrolle@univ-lille.fr)

Abstract.

Formation of Ultrafine particles (UFPs) in the urban atmosphere is expected to be less favored than in the rural atmosphere due to the high existing particle surface area acting as a sink for newly-formed particles. Despite the large condensation sink (CS) values, previous comparative studies between rural and urban site reported higher frequency of new particle formation (NPF) events over urban sites in comparison to background sites as well as higher particle formation and growth rates attributed to the higher concentration of condensable species. The present study aims to better understand the environmental factors favoring, or disfavoring, atmospheric NPF over Lille, a large city North of France and to analyze their impact on particle number concentration using a long-term dataset (4 years : 1st July 2017 to 31st December 2020).



The results highlight a strong seasonal variation of the NPF occurrences with a maximum observed during spring (27 events) and summer (53 events). It was found that high temperature ($T > 295\text{K}$), low RH ($\text{RH} < 45\%$) and high solar radiation are ideal to observe NPF events over Lille. Relatively high values of condensation sink ($\text{CS} \sim 2 \cdot 10^{-2} \text{ s}^{-1}$) are reported during event days suggesting that high CS does not inhibit the occurrence of NPFt over our site. Moreover, the particle Growth Rate ($\text{GR}_{15.7-30\text{nm}}$) was positively correlated with the temperature most probably linked to the higher emissions of precursors. Finally, the nucleation strength factor (NSF) was calculated to highlight the impact of those NPF events on particle number concentrations. $\text{NSF}_{15.7-100}$ reaches a maximum of 4 in summer, indicating an enormous contribution of NPF events to particle number concentration at this time of the year.

1 Introduction

New Particle Formation (NPF) leads to the formation of a large number of sub-20nm particles that will contribute to the levels of fine particles observed in ambient air. The latter can have adverse effect on human health as they can penetrate deeply into the pulmonary system (Clifford et al., 2018; Ohlwein et al., 2019). The freshly-formed particles then grow to larger sizes, from a few nm in particle diameter up to sizes ($\text{Dp} > 100 \text{ nm}$) at which they may act as cloud condensation nuclei (CCN, (Pierce and Adams, 2009; Ren et al., 2021; Rose et al., 2017; Spracklen et al., 2006). NPF events have been observed around the world (Kerminen et al., 2018; Kontkanen et al., 2017; Kulmala et al., 2004) in various environments from the boundary layer (BL) at urban locations (Ganguly and Jayaraman, 2006; Roig Rodelas et al., 2019; Tuch et al., 2006; Wehner and Wiedensohler, 2003) as well as remote polar background areas (Dall'Osto et al., 2018) but also within the free troposphere (Rose et al., 2015b, 2015a). NPF events are typically associated to a photochemical origin, thus occurring mostly during daytime (Kulmala et al., 2014), with some scarce events being observed during nighttime (Roig Rodelas et al., 2019; Salimi et al., 2017).

NPF occurrence depends on various factors including precursor emission strength, number concentration of pre-existing aerosol population, meteorological parameters (in particular solar radiation, temperature



51 and relative humidity) and oxidation capacity of the atmosphere (Kerminen et al., 2018). Differences were
52 found in both the seasonality and intensity of NPF events according to the site type (urban, traffic, regional
53 background, rural, polar, high altitude (Dall'Osto et al., 2018; Sellegri et al., 2019). This variability seems
54 to be related to the environmental conditions that are specific to each location, which makes it hard to
55 draw general conclusions on the conditions that trigger NPF events (Berland et al., 2017; Bousiotis et al.,
56 2021). However, Nieminen et al. (2018) highlighted a common seasonal occurrence of NPF during spring
57 and summer using datasets from 36 continental sites worldwide.

58 The formation and growth of initial clusters to detectable sizes ($D_p > 1\text{-}3\text{ nm}$) compete with their
59 simultaneous removal from the ultra-fine particle mode by coagulation with pre-existing particles
60 (Kerminen et al., 2001; Kulmala, 2003). Because of this, the number concentration of particles smaller
61 than 20 nm has been observed to be anti-correlated with the aerosol volume and mass concentration over
62 rural area in Northern Italy (Rodríguez et al., 2005). Indeed, the total aerosol volume is rather small during
63 nucleation events (Kerminen et al., 2018; Rodríguez et al., 2008). While the negative effect of increased
64 pre-existing particle surface area (often described with the condensation sink, CS) on the occurrence of
65 these events is widely accepted (Kalkavouras et al., 2017), yet cases are found when NPF events occur
66 on days with higher CS compared to average conditions (Größ et al., 2018; Kulmala et al., 2017).

67 A recent study (Bousiotis et al., 2021) using large datasets (16 sites) over Europe (6 countries) highlighted
68 that solar radiation intensity, temperature, and atmospheric pressure had a positive relationship with the
69 occurrence of NPF events at the majority of sites (exceptions were found for the southern sites), either
70 promoting particle formation or growth rate. Indeed, solar radiation is considered one of the most
71 important factors in the occurrence of NPF events, as it contributes to the production of NPF precursors.
72 Higher temperatures are considered favorable for the growth of newly formed particles as they can be
73 linked to increased concentrations of organics vapor (Wang et al., 2013) that support particle but also
74 reduce the stability of the initial molecular clusters (Deng et al., 2020; Kurtén et al., 2007).

75 The wind speed, on the other hand, has presented variable effects on the occurrence of NPF events results,
76 appearing to depend on the site location rather than their type (Bousiotis et al., 2021). Additionally, the
77 origin of the incoming air masses plays a very important role, since air masses of different origins have
78 different meteorological, physical and chemical characteristics. Therefore, the probability of NPF event



79 occurrence at a given location and time depends not only on local emissions, but also on long range
80 transport (Sogacheva et al., 2007, 2005; Tunved et al., 2006) and on synoptic meteorological conditions
81 at the European scale (Berland et al., 2017).
82 Formation of new particles in the urban atmosphere is expected to be less favored than in the rural
83 atmosphere due to the high existing surface area of particles acting as a sink for freshly-formed particles.
84 Despite the large CS values, previous comparative studies between rural and urban site reported higher
85 frequency of NPF events (Peng et al., 2017) over urban sites in comparison to background sites as well
86 as higher particle formation and growth rates (Niemininen et al., 2018; Salma et al., 2016; Wang et al.,
87 2017) attributed to the higher concentration of condensable species. This study presents the first
88 observations of new particle formations over Lille, a large city in the north of France. Based on a multi-
89 annual dataset (2017-2020), the frequency and intensity of the events are analyzed aiming to better
90 constrain the favorable and unfavorable conditions.

91

92 **2 Materials and methods**

93 The ATOLL (ATmospheric Observations in LiLLE) station is located in Villeneuve d'Ascq, Northern
94 France (50.6114 N, 3.1406 E), and only 4 km away from the city center of Lille, which is the core of the
95 metropolis (Métropole Européenne de Lille, more than 1.1 million inhabitants) to which Villeneuve
96 d'Ascq belongs. Observations such as low Single Scattering Albedo (SSA) values (0.75 on average within
97 the PM₁ fraction, Velasquez-Garcia et al., under review) and large particle number concentrations (6140
98 cm⁻³ on average) suggest that aerosol measurements performed at ATOLL aerosol conditions are
99 comparable to GAW sites classified as urban (Laj et al., 2020). ATOLL is also part of ACTRIS (Aerosols,
00 Clouds, and Trace gases Research InfraStructure Network, <http://www.actris.net>) program,
01 complementing the high-quality long-term atmospheric data in Northern France. This station is under the
02 influence of many anthropogenic sources, e.g. road traffic, residential sector, agriculture and industries
03 (Chen et al., 2022), as well as maritime emissions, and more episodically under the influence of events of
04 aged volcanic plumes and desert dust (Bovchaliuk et al., 2016; Mortier et al., 2013).

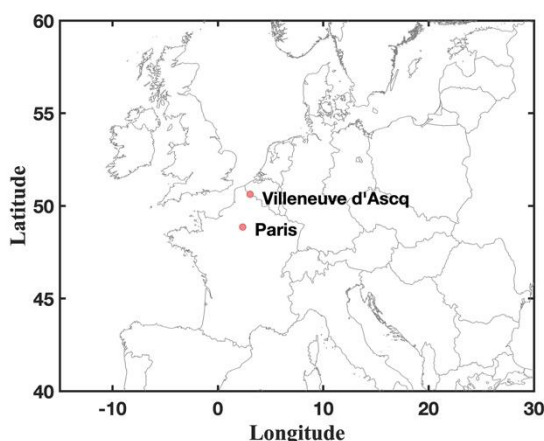


Figure 1 : ATOLL location in Villeneuve d'Ascq (Northern France) and picture of the station on the rooftop of the University of Lille P5 building (© LOA).

A large set of *in-situ* and remote sensing instruments are implemented in ATOLL to characterize physical, chemical, optical and radiative properties of particles and clouds. *In-situ* instruments have independent sampling stainless-steel lines located at least 1 meter above the roof top and equipped either with PM₁ cyclone or PM₁₀ inlet. The measurements used for that study were performed between 1st July 2017 and 31st December 2020. The instruments use in this study focused on aerosol properties including number size distributions, chemical composition, and optical properties, and details are described below.

The Scanning Mobility Particle Sizer (SMPS) measures particle number size distribution between 15.7-800 nm. The SMPS system consisted of a TSI model 3775 condensation particle counter, a TSI 3082 – type differential mobility analyzer (DMA) as described by (Villani et al., 2007) and a Nickel aerosol neutralizer (Ni-63 95MBq). The sheath flow rate was controlled with a critical orifice in a closed loop arrangement (Jokinen and Mäkelä, 1997). Typically, the scan time was chosen to be 300 seconds. To take into account the multiple charge effect and the losses through diffusion, particle concentrations were corrected using the equation given by the manufacturer specifications (AIM 10.2.0.11).



21 Accordingly, aerosol number size distribution data from the SMPS measurements were used to classify
22 individual days as NPF event, undefined or non-event days. The classification followed the procedure
23 presented in (Dal Maso et al., 2005) following the decision criteria based on the presence of fine particles
24 ($D_p < 25$ nm) and their consequent growth to Aitken mode. Briefly, event days are identified when sub-
25 25nm particle formation and growth are observed. On non-event days nucleation mode is absent. Finally,
26 undefined days are the days when sub-25nm particles are observed but do not grow subsequently or last
27 less than an hour.

28 SMPS dry (using a Nafion) particle number size distributions were also used for CS and growth rate (GR)
29 calculations. The CS estimates the loss rate of the condensable vapors (Kulmala et al., 2001) which were
30 assumed to have molecular properties similar to sulfuric acid for CS calculation (Dal Maso et al., 2005).
31 A high CS indicates the presence of large surface area of aerosol particles onto which NPF precursors can
32 condensate and particles can coagulate as well. The particle GR was calculated based on the maximum-
33 concentration method described in (Kulmala et al., 2012). First, the NPF starting time was identified when
34 the newly formed mode was observable in the first bins of the SMPS (15.7 nm) and the time of peak
35 concentrations for particles with diameter of 30 nm (N_{30}) during NPF were manually identified. Particle
36 $GR_{15.7-30}$ was then calculated by linear regression of particle size vs. time span from the NPF start until
37 time when N_{30} reaches a maximum.

38 Absorption coefficients (σ_{abs}) were continuously measured with a seven-wavelength aethalometer (AE33,
39 Magee Scientific Inc., Cuesta-Mosquera et al., 2020). According to ACTRIS current guidelines
40 (<https://actris-ecac.eu/particle-light-absorption.html>), σ_{abs} coefficients at each wavelength have been
41 recalculated by 1) multiplying equivalent Black Carbon (eBC) by the mass-specific absorption coefficient
42 (MAC) and then 2) dividing by the suitable harmonization factor to account for the filter multiple
43 scattering effect, i.e. 2.21 (M8020 filter tape) in 2017 and 1.76 (M8060 filter tape) afterwards. The
44 aethalometer samples at $5 \text{ L} \cdot \text{min}^{-1}$ downstream a PM_{10} cyclone (BGI SCC1.197, Mesa Labs). The spectral
45 dependency of σ_{abs} was used to determine the contributions of traffic (fossil fuel - FF) and Wood Burning
46 (WB) to eBC via a source apportionment model (Sandr Dewi et al., 2008).

47 Meteorological data including temperature, water vapour mixing ratio, and solar radiation were also
48 measured every minute at the sampling site using a weather station (DAVIS Inc weather station, Vantage



Pro 2) and a set of Kipp and Zonen pyranometer (CM22), pyrheliometer (CH1) and pyrgeometer (CGR4). A skyimager (Cloudcam, CMS) was also used to estimate the sky cloudiness (Shukla et al., 2016). Three-day air mass backtrajectories of air masses arriving at ATOLL at half the boundary layer height between July 1, 2017 and December 31, 2020 were computed every hour using the Hybrid Single-Particle Lagrangian Integrated Trajectory (HYSPLIT version 5.1.0) transport and dispersion model from the NOAA Air Resources Laboratory (ARL) (Rolph et al., 2017; Stein et al., 2015) and meteorological input from the Global Data Assimilation System (GDAS) at $1\times 1^\circ$ resolution, resulting in 30719 backtrajectories.

3 Results

3.1 NPF event frequency and Growth rate

The seasonal distribution of NPF events at the ATOLL site is displayed in Figure 2. SMPS missing data (in Figure 2) are about 40% from January to April due to the yearly calibrations at the manufacturer premises and few laboratory campaigns (Oct 2018 – Jun 2019). Over the 4 years of measurements (2017-2020), 96 (11%) days were classified as NPF events, 355 (40%) as undefined days and 432 (49%) as non-event days. One can also note that most of the NPF events identified at the ATOLL site were observed during spring (March-April-May, 27 events corresponding to 15% of the days when observations were available during this season) and summer (June-July-August, 53 events corresponding to 19%) with a maximum observed in June consistent with a previous study over central Europe (Dall'Osto et al., 2018). During winter, the number of events is extremely limited (only one event observed in February). In the following sections, only observations from spring and summer seasons will be discussed due to the low representativeness of NPF events in fall ($n=15$) and winter ($n=1$). Moreover, the undefined event days are seen all year round (frequency around or larger than 20%) with a clear peak in August (frequency at 62.5%) consistent with observations over boreal forest where undefined days were also observed to be most frequent in early fall (Mazon et al., 2009).

Using long-term measurements from 36 sites (polar, rural, high altitude, remote, urban), Nieminen et al., (2018) reported an annual NPF frequency below 15% for half of the sites (18 sites from all types) and



occasionally over 30% for 10 sites. Moreover, they highlighted a seasonal variation of NPF occurrence with larger (lower) frequency, about 30 % (10%), during spring (winter). Frequency analysis of NPF occurring only over urban or anthropogenically influenced sites show large site-to-site differences for all seasons. Indeed, NPF occurrence frequencies are varying from 20% (Helsinki in Finland, Sao Paulo in Brazil) to 80% (Beijing in China, Marikana in South Africa) during spring and from 7% (Helsinki) to 78% (Marikana) during winter. Yearly average of NPF occurrence frequencies are between 11% (Helsinki) and more than 60% (Beijing and Marikana).

The ATOLL event frequency (seasonal variation and values) is similar to observations performed in Paris (Dos Santos et al., 2015) while the frequency of undefined and non-event days are quite different. Indeed, in Paris the non-event frequency is larger than 60% except in July and August whereas over ATOLL the non-event frequency shows a clear seasonal pattern with lower frequency (<40%) from April to August. Moreover, undefined event frequency in Paris shows a minimum (<5%) in May and June and remains quite steady during the rest of the year (around 20%). One can note that the frequency of undefined events (also considered as failed events) is much higher over ATOLL all year long with an average of 40% while it remains below 40% over the boreal forest. The frequency of undefined events observed at ATOLL is clearly larger than the frequencies observed over more polluted site (Paris) and a pristine site (Boreal forest). This might show that ATOLL is under the influence of air masses or particle and precursor sinks that favor the burst of UFP.

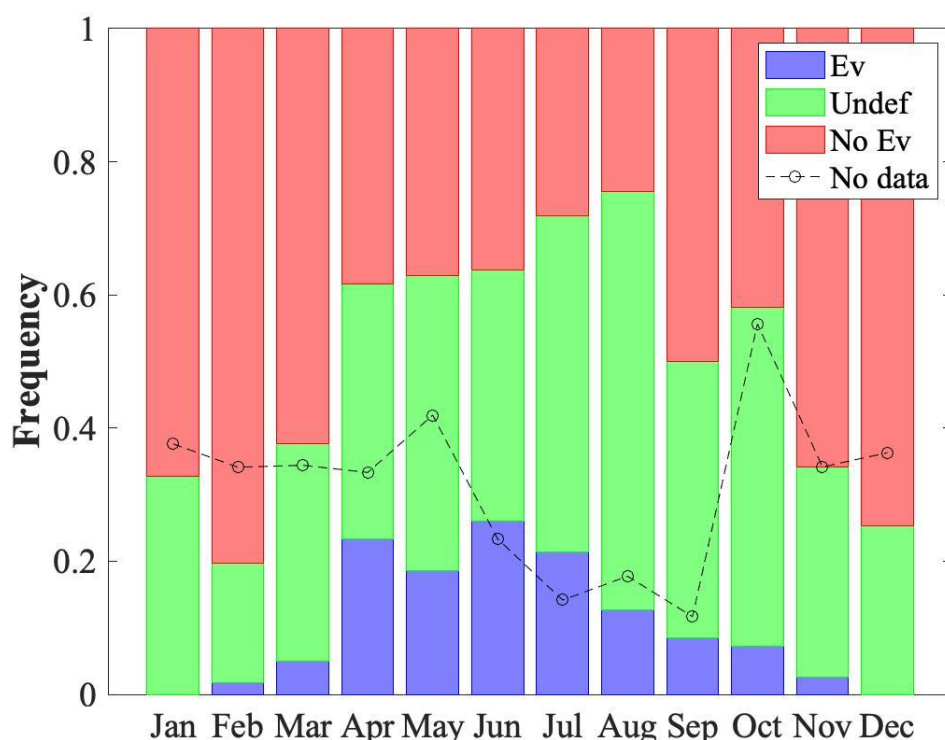


Figure 2 : Seasonal distribution of event days (blue), undefined days (green), and non-event (red) days at the ATOLL station, Lille, France, during 2017–2020. Days with missing data are excluded from the total number of days per month and the frequency of missing data are indicated with the black circles.

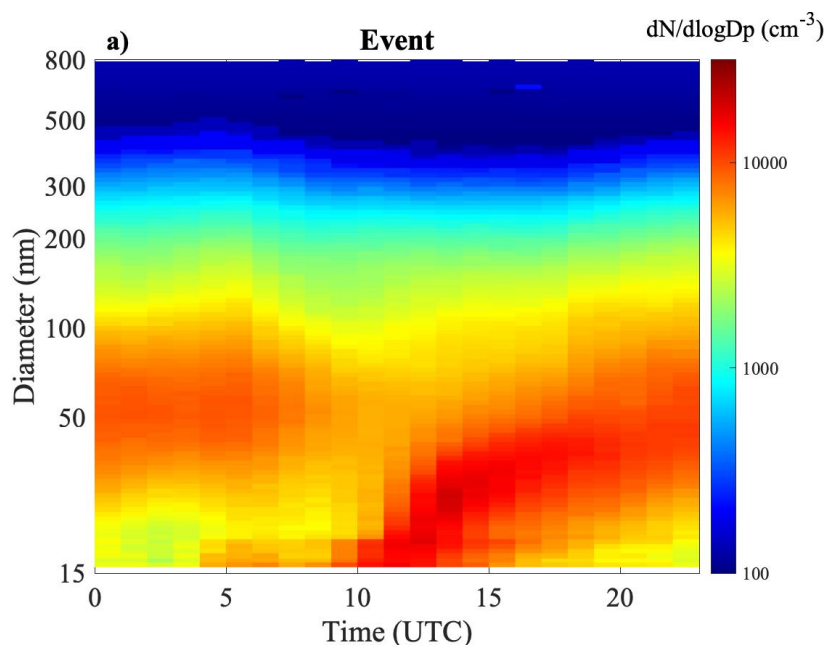
96

97 3.2 Aerosol dry size distribution

98 Median daily contour plots of the particle number size distributions (PNSD) obtained from the SMPS are
 99 shown in Figure 3 separately for NPF event, undefined and non-event days observed during the warm
 00 period (only spring and summer). Atmospheric NPF and subsequent particle growth are seen in Figure 3a
 01 as an emergence of new aerosol particles with small diameter followed by the growth of these particles
 02 into larger sizes. If this phenomenon is taking place regionally (few tens of km in radius), a so called
 03 ‘banana plot’ is observed in particle number size distributions as a function of time at a fixed location.



04 The time evolution of the “median NPF day” (Figure 3a) displays a similar growth pattern for newly
 05 formed particles than for individual NPF event days (See supplementary materials). Indeed, one can
 06 clearly see a UFP mode appearing from 10:00 to 15:00 (UTC) and growing during the rest of the day.
 07 The NPF starting time and the growth rate will be discussed in the following section. By 23:00 UTC, the
 08 newly formed particles reach an average diameter of 50 nm, similar to the geometric diameter of the mode
 09 of the pre-existing particles observed during the morning (00:00 – 08:00). The “median undefined day”
 10 (Figure 3b) highlights a burst of UFP from 10:00 to 15:00 (UTC) that is not growing and does not last
 11 during the whole afternoon. The behavior of the median is again similar to the individual undefined
 12 events observed during this period. The “median non-event day” (Figure 3c) shows no sign of particle
 13 growth, as expected.



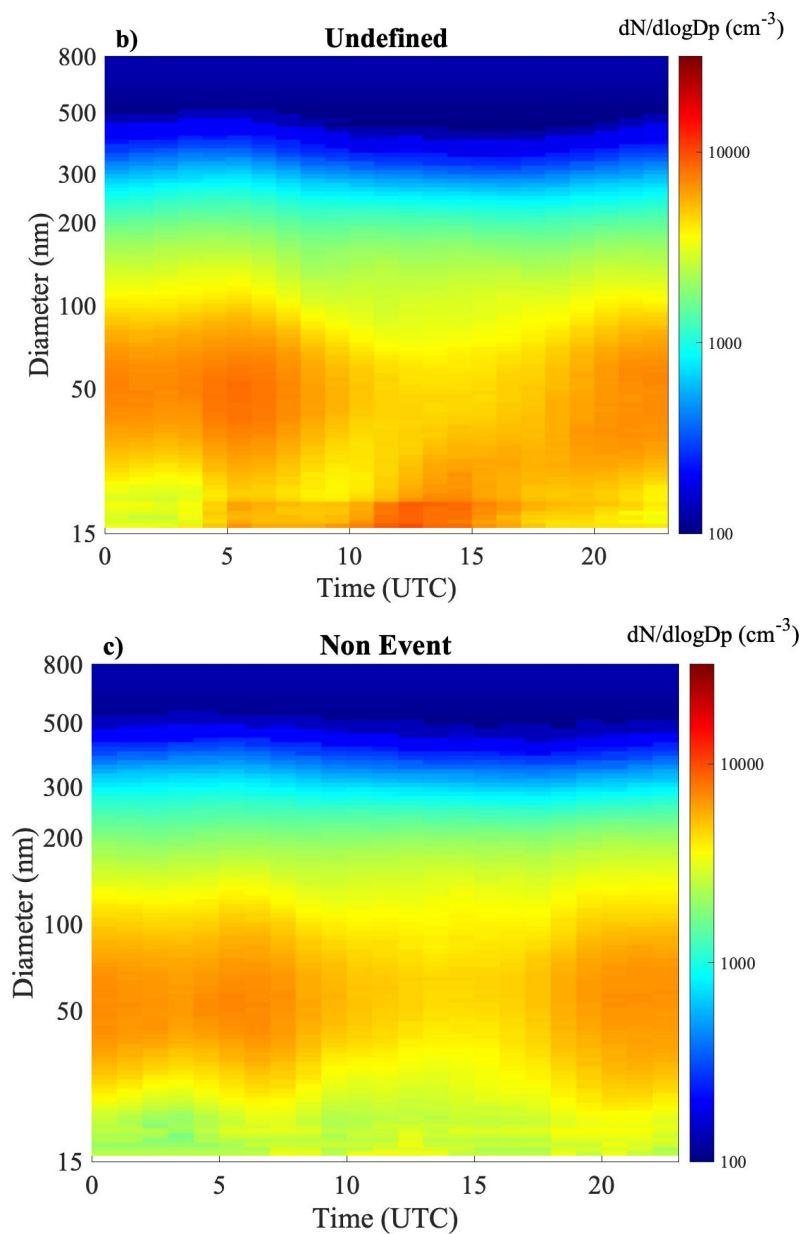


Figure 3 : Median particle number size distribution (15.7 nm < Dp < 800 nm) observed during NPF event (a), undefined (b) and non-event (c) days in spring and summer from 2017-2020.



3.3 Starting time and Growth rate

Figure 4 shows the monthly variation of the starting time and growth rate of each event observed at ATOLL. Most NPF events observed in ATOLL were observed to start between 09:00 and 14:00 local time (74%), with fewer events in the early morning (07:30 - 09:00, 6%) and late afternoon (15:00 and 19:30, 20%). NPF starting time as well as GR strongly depend on the month during which the event is observed. Indeed, the NPF starting time becomes earlier during the colder period and reaches a minimum in June (around 08:20). No NPF event were observed after 16:00 in summer. During spring and fall, the average NPF starting time varies between 10:00 and 19:00. Nocturnal events are rarely observed, with only one occurrence in August. The start time monthly variability is linked to sunrise and sunset times. In the following section, a link between the total solar irradiation and NPF occurrence will be examined. The event ending time was determined as the time when the growth of the freshly formed particles was over, i.e. when the diameter reached the diameter of the pre-existing particles. The duration of nucleation events, at ATOLL, was then estimated and varies from an hour up to 28 hours. On average, NPF duration is shorter from May to August (around 8 hours) and increases up to around 13 hours on average during colder months (March and November). This seasonal behavior could be due to the presence of availability of condensable vapors, air mass origin, and environmental conditions favorable to NPF events (see section 3.2).

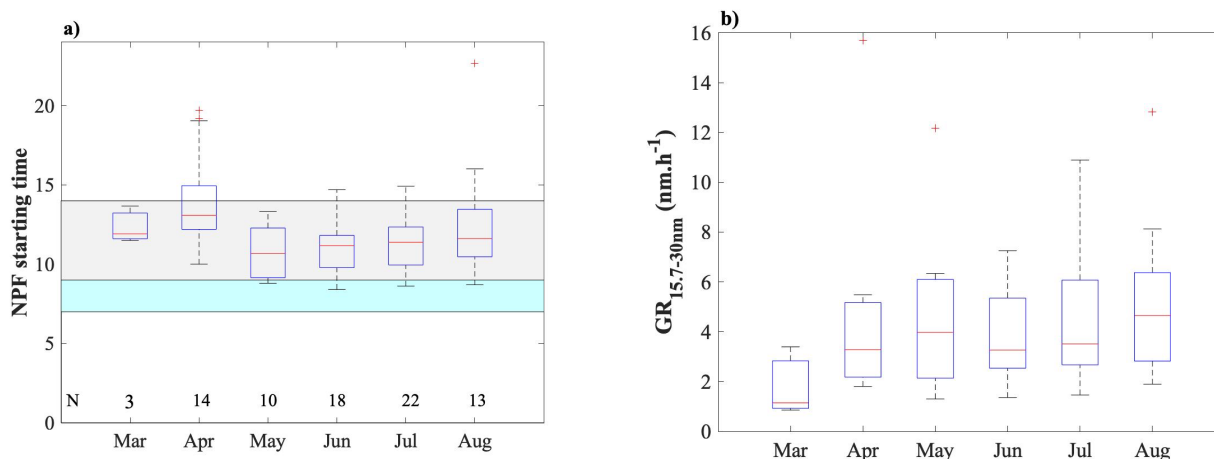




Figure 4 : Monthly variation of new particle formation starting time (a) and their Growth Rate ($GR_{15.7-30nm}$) at the ATOLL station during 2017–2020. The grey area represents the period, from 09:00–14:00, when most of the NPF events occur. The blue area corresponds to the period before the NPF onset (07:00– 09:00). N represents the number of events observed per month.

The growth rate values ($GR_{15.7-30nm}$) observed at ATOLL lie within 0.8 to 15.7 $nm.h^{-1}$ and show a strong monthly variation with the lowest values observed in spring and fall and the largest ones observed during summer (Figure 4). $GR_{15.7-30nm}$ values were in addition plotted as a function of temperature for all years and seasons in Figure 5, which highlights that below 20°C, $GR_{15.7-30nm}$ values are lower than 6 $nm.h^{-1}$, while, under warmer conditions ($T > 20\text{ °C}$), $GR_{15.7-30nm}$ reach values up to 16 $nm.h^{-1}$. These results show a clear temperature dependance of the particle growth. Indeed, higher temperatures have been shown to favor emission of biogenic precursors, including monoterpenes known to favor the occurrence of NPF events (Kulmala et al., 2004). Previous studies (Paasonen et al., 2018; Yli-Juuti et al., 2011) have shown that the GR usually has larger values during warm periods and especially during summer. Over urban areas (Beijing or Shanghai), $GR_{15-25nm}$ showed no clear seasonal variation (Yao et al., 2018). However, recent studies also have highlighted the link with GR seasonal pattern and high abundance of biogenic volatile organic compounds during warmer periods over boreal forest (Paasonen et al., 2018; Yli-Juuti et al., 2011). Therefore, the observed seasonal variation of GR values may be related to temperature variation that influences the emissions of organic compounds in the atmosphere (Figure 5).

As previously observed in Figure 3a, the mean geometric diameters reached by the end of all NPF events are similar and averaged around 50 nm. This can be explained by the presence of a pre-existing mode of particles centered around 50 nm. Moreover, the seasonal variation of the NPF event duration could be then linked to the $GR_{15.7-30nm}$ seasonal variation. As the final diameter is similar in all cases, the lower the $GR_{15.7-30nm}$ values will then be associated with the longer NPF duration. The seasonal variation of NPF duration highlighted earlier is then only a consequence of the GR seasonal variation.

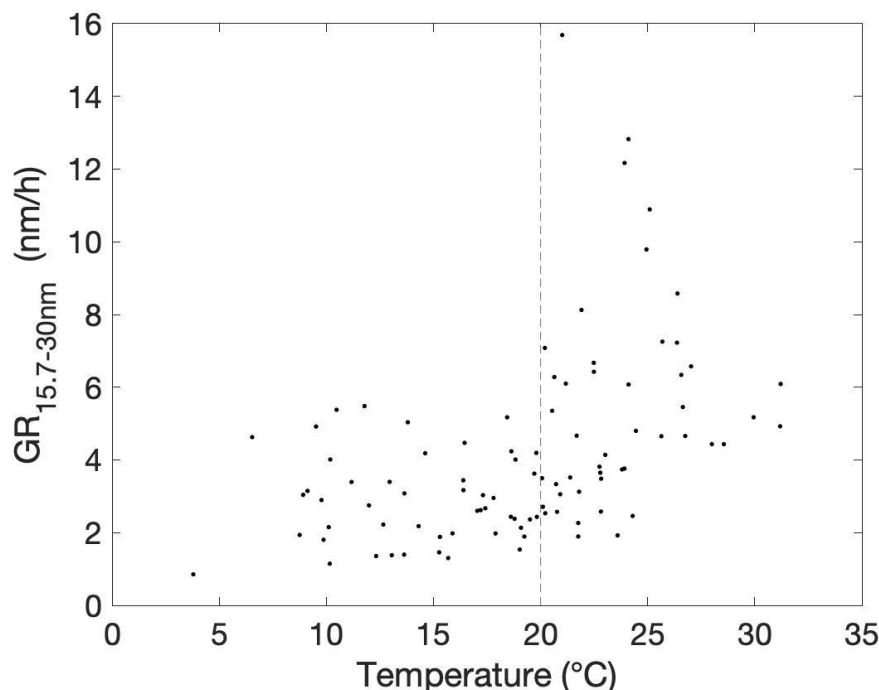


Figure 5 : Growth rate values ($GR_{15.7-30nm}$) as a function of ambient temperature.

35

36 3.4 Environmental conditions

37 The effect of cloudiness on NPF event occurrence is shown in Figure 6a, with a specific focus on
 38 measurements collected between 09:00 and 14:00, i.e. the period of time where most NPF tended to start.
 39 The cloud fraction was calculated from the sky imager dataset following the method by (Shukla et al.,
 40 2016) and sorted as a function of event, undefined and non-event days. There is a clear inverse correlation
 41 between cloud fraction and NPF occurrences. Average cloud fraction is around 0.47 during event days,
 42 0.68 during undefined days and 0.74 during non-event days. Moreover, the 25th percentiles of the cloud
 43 fractions for event, undefined and non-event days, respectively 0.06, 0.47, 0.63, clearly show that the
 44 absence of clouds (lower cloud fraction) is mostly associated with NPF events. This result is consistent
 45 with previous analysis performed over the boreal forest (Dada et al., 2017) and is linked to the fact that
 46 radiation seems essential for NPF during the warmer period, as the events occur almost solely during



daylight hours (Kulmala et al., 2004). Figure 6b shows the average diel total solar radiations observed during events, non-event and undefined days for spring and summer. As expected, total solar radiation is on average always larger during event days in comparison to non-event days, with a more pronounced difference observed during spring.

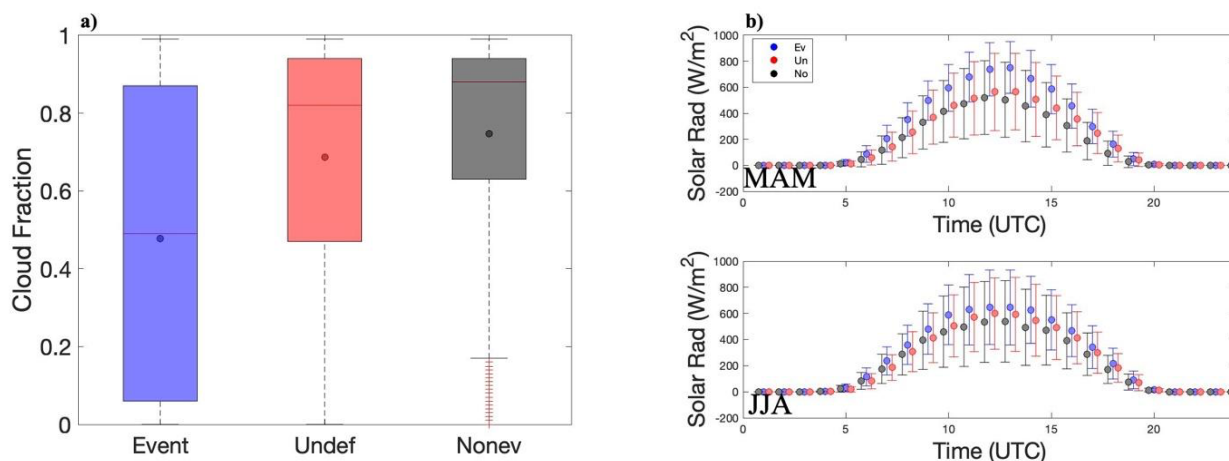


Figure 6 : (a) Cloud fraction observed from 09:00 to 14:00 UTC during event, undefined and non-event days. The red line represents the median while the lower and upper edges of the box represent the 25th and 75th percentiles, respectively. The lower and upper edges of the whisker represent 10th and 90th percentiles, respectively. The circles represent the average. (b) Diel variations (UTC) of the mean total solar radiation observed during the event days (blue), undefined days (green) and non-event days (red) during spring (MAM, top) and summer (JJA, bottom) seasons (b). The error bars correspond to one standard deviation.

Other environmental parameters known to influence the occurrence of NPF events, such as temperature and humidity were also sorted to highlight diel and seasonal variations (Figure 7). Our results (Figure 7a) indicate that NPF is favored by low values of ambient relative humidity, especially during spring, consistently with previous studies (Duplissy et al., 2016; Hamed et al., 2011; Merikanto et al., 2016). A few reasons can explain this tendency: (1) high RH values ($RH > 90\%$) observed at the surface are usually associated to the presence of low altitude clouds reducing incoming total radiation and then preventing NPF formation, (2) at moderately high RH ($RH > 40\%$), hydrophilic aerosols could grow which will enlarge the sink for precursors and (3) high RH values limit some VOC (Volatile Organic Compounds)



60 ozonolysis reactions, which further prevents the formation of condensable vapors necessary for nucleation
 61 (Boy and Kulmala, 2002).
 62 Figure 7b shows the diel median temperature conditions (T) during NPF events, nonevents and undefined
 63 days. NPF events occurred within temperatures ranging between 3° C and 33.5°C. During both seasons,
 64 averaged temperatures during event days are always larger than during non-event days, with, again larger
 65 differences during spring. One should note that days with high temperatures in spring and summer are
 66 usually also days with high solar radiation, consistently with conclusions from Figure 6. The temperature
 67 difference between undefined days and event days is clearly marked during spring and fade away during
 68 summer. As previously discussed, higher temperatures favor emission of biogenic precursors, including
 69 monoterpenes known to favor the occurrence of NPF event (Kulmala et al., 2004). However, high
 70 temperature can also lead to evaporation of molecular clusters which may inhibit NPF events (Dada et
 71 al., 2017; Deng et al., 2020).

72

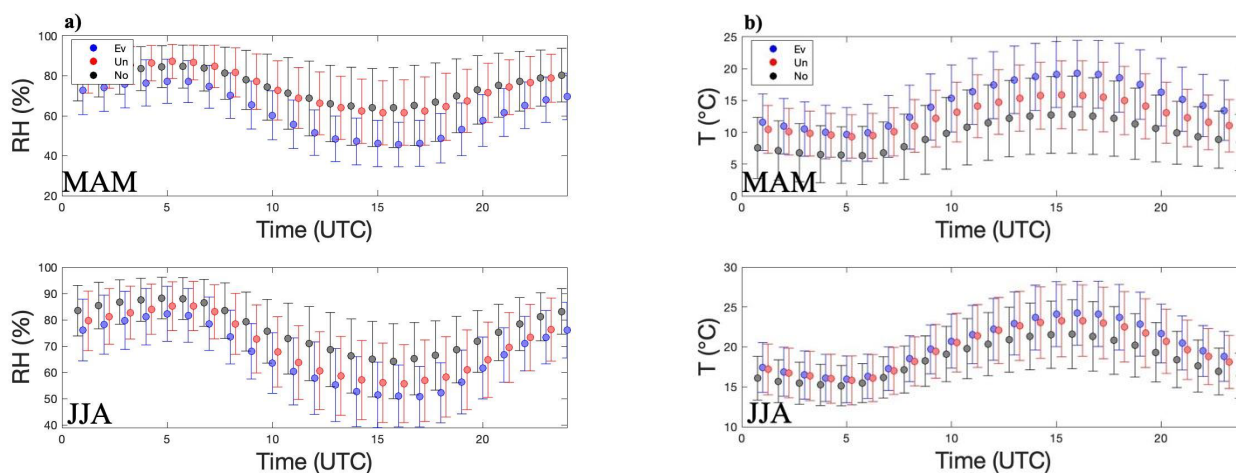


Figure 7 : Diel variation (UTC) of mean Relative Humidity (RH, a) and mean temperature (b) observed during the event days (blue), undefined days (green) and non-event days (red) during spring (MAM) and summer (JJA) seasons. The error bars correspond to one standard deviation.



3.5 Condensation sink

The CS characterizes the loss rate of atmospheric vapors to aerosol particles. The diel variations of CS calculated for spring and summer and for NPF event, undefined and non-event days are shown in Figure 8a. Averaged CS values are high (larger than $2 \cdot 10^{-2} \text{ s}^{-1}$) during event days occurring during spring and summer (Figure 8a). During NPF event days and over different urban sites (Beijing, Nanjing or Hong Kong), CS values ranging from 0.6 up to $10.7 \cdot 10^{-2} \text{ s}^{-1}$ were reported (Xiao et al., 2015). Over pristine sites, such as Hyytiälä, the CS values are between $0.05 - 0.35 \cdot 10^{-2} \text{ s}^{-1}$. As events occur anyway, low values of CS, often considered as the major limiting factor in the NPF occurrence do not inhibit the occurrence of NPF events in ATOLL consistently to previous observations in similar environments, such as Melpitz observatory (Größ et al., 2018) or over Chinese megacities (Xiao et al., 2015). One can assume that the presence of large concentrations of precursors could explain the formation of particles over polluted sites such as ATOLL. Unfortunately, precursors were not measured over the 4-year period of interest here therefore this assumption would require further investigation beyond the scope of this study.

In the afternoon, CS during event days increases due to the growth of freshly emitted particles, especially during summer. Contribution of newly formed particles ($D_p < 50 \text{ nm}$) to the CS is about 36% and 27%, during summer and spring respectively, while the contribution of pre-existing particles ($D_p > 150 \text{ nm}$) to the CS is below 20% for both seasons. Moreover, during non-event days, the size resolved median CS is shifted to larger particle diameters with a maximum observed around 100 nm for all seasons.

To evaluate the impact of the background CS on NPF occurrence, all CS values observed from 07:00-09:00, period before NPF starting time (green area on Figure 4a), were averaged during event, non-event and undefined days. It was found that the total CS_{07-09h} was larger (around 16%) during non-event days in comparison to undefined and event days. Moreover, this difference is mostly due to particles larger than 70 nm according to size resolved CS_{07-09h} (Figure 8b). The difference between non-event and event days is lower than what is usually observed over pristine sites (Lyubovtseva et al., 2005) but significant enough to trigger the NPF event occurrence.

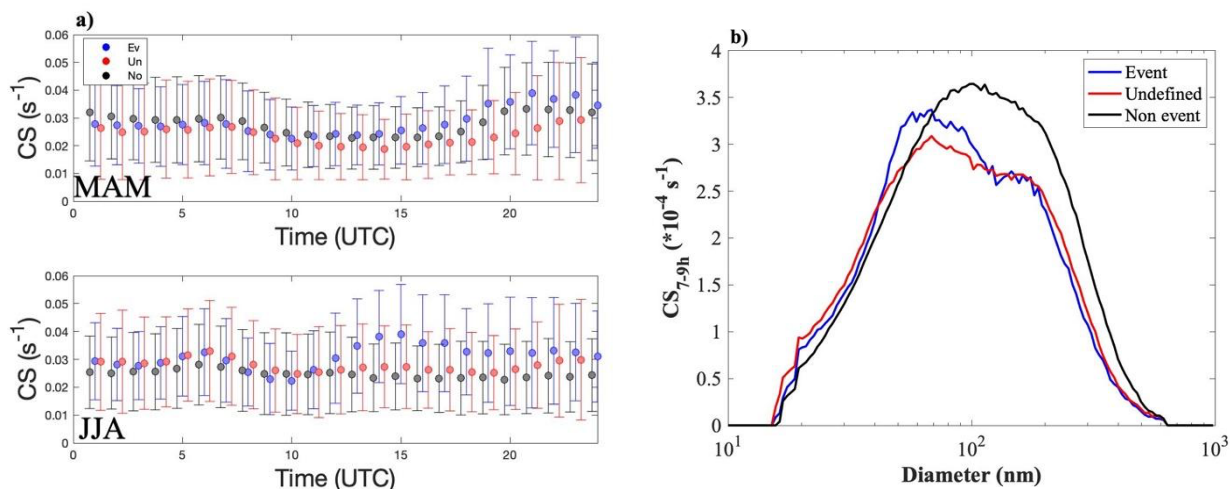


Figure 8 : (a) Diel variation of Condensation Sink (CS) during spring (MAM) and summer (JJA) seasons. (b) Median size resolved CS for MAM and JJA during event days (blue), undefined (red) and non-event days (black).

Additionally, the correlation coefficients between meteorological parameters and pollutants (gas and particles) are reported in Table 1 for the entire period of measurements (all seasons). Hourly average over a time window between 09:00 - 14:00 (NPF event starting time period) of few variables (total CS, T, RH and BC_{wb}) were used to calculate those correlation coefficients (corresponding to 7025 and 35433 data points for NPF event and Non-event days, respectively).

The correlation of Black Carbon from wood burning (BC_{wb}) during non-event days with the condensation sink is high ($R = 0.67$). This correlation between these parameters is clearly absent during event days ($R = 0.19$). One can also note that NO_x concentrations have a positive correlation (0.30) with CS during NPF non-event days while the same correlation is negative (-0.17) during NPF event days. The NO_x sources over urban area are mostly anthropogenic (house heating, traffic and industries) sources which is consistent with its relatively high correlation coefficients with BC_{wb} (0.47 and 0.65). As highlighted in (Barreira et al., 2020), BC_{wb} and NO_x are evolving through the year showing a minimum in summer and a maximum in winter when sources are stronger due to colder temperatures and residential heating



emissions. As non-event days are mostly (62%) observed during cold months and NPF events are largely (82%) observed during warmer months, the correlation between BC_{wb} , NO_x and CS during non-event is not surprising. However, during spring, air masses observed during NPF events are clearly “cleaner” (in terms of NO_x and BC_{wb}) than non-event cases. Indeed, NO_x and BC_{wb} concentrations are lowered by 18% and 36% respectively during spring NPF event days in comparison to non-event days. During summer, NO_x and BC_{wb} concentrations reach an annual minimum and there both pollutant concentrations are similar between NPF event and non-event days (lowered by -0.04% and 0.01% during NPF event days).

Table 1 : Correlation coefficients between different meteorological parameters (T, RH), Nitrogen oxide (NO_x), Black carbon concentrations (BC_{wb} from wood burning) and total condensation sink during event and non-event for the 4 years period (2017-2020) and in a time window (09:00 – 14:00). High positive or negative correlations are marked in bold.

		CS	T	RH	NO_x	BC_{wb}
Event days	CS	1				
	T	0.55	1			
	RH	-0.39	-0.40	1		
	NO_x	-0.17	-0.24	0.48	1	
	BC_{wb}	0.19	-0.04	0.11	0.47	1
Non- event days	CS	1				
	T	0.06	1			
	RH	-0.03	-0.50	1		
	NO_x	0.30	-0.44	0.44	1	
	BC_{wb}	0.67	-0.37	0.28	0.65	1

Moreover, during event days the temperature is positively correlated (0.55) with the CS, while, during non-event days, this correlation is clearly not observed during non-event days (0.06). Over boreal forest,



CS and temperature are correlated during event day (Liao et al., 2014). Indeed, this coupling comes from the enhanced growth of particles due larger monoterpene emissions at higher temperature, which naturally leads to higher concentration of larger particles and thus higher CS. As the particle growth during event days is clearly related to temperature increase (Figure 5) most probably due to higher concentration of condensable gasses, it is not surprising to observe this temperature and CS coupling.

3.6 Air mass trajectories

One can note that environmental conditions (CS, Temperature and RH) observed during undefined events are mostly between event and non-event days. A deeper analysis on undefined days reveals that on these days, particle growth stopped due to (i) a decrease of the total irradiance due to a cloud passage over the site (20% of cases), (ii) a shift of the wind direction (17% of cases), (iii) or both parameters changing simultaneously (35% of cases).

The shift of the wind orientation leading to a stop of the particle growth indicates that NPF events are associated with certain wind directions or air mass origins. To investigate this, HYSPLIT back trajectories were first sorted as a function of event, non-event and undefined days. Only the back-trajectories arriving between 09:00-14:00 (period of NPF high occurrences) were selected for further analysis. During the NPF events, the predominant air masses were tracked back along the Eastern North Sea region. Comparing these results to back trajectories during non-event days highlight more continental influence. Indeed, most of the back trajectories during non-event days pass over large cities (Dunkirk, Paris, London, Rotterdam) before reaching Lille metropolis. Those air masses might then have been slightly enriched in pre-existing particles larger than 100 nm ($CS_{7_{9h}}$ slightly larger (16%) during non-event days) which would decrease the occurrence of NPF events in Lille or could have been depleted in precursor vapors. This result is consistent with previous results showing “cleaner” air masses are associated with NPF event cases observed during spring.

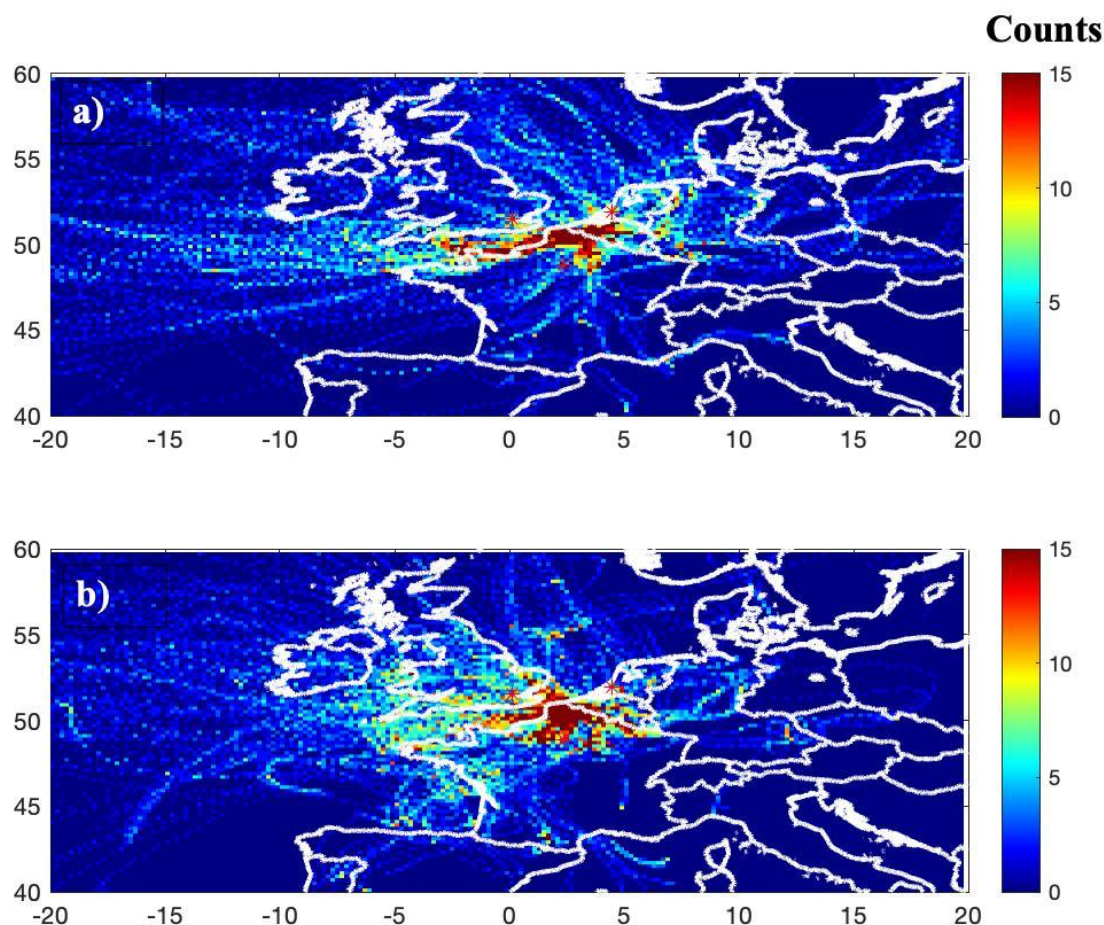


Figure 9 : 3 days hourly back trajectories arriving in ATOLL between 09:00-14:00 UTC during (a) new particle formation (NPF) events and (b) non-events days. The back trajectories were calculated for each hour at ATOLL at half the boundary layer height. The color contour represents the back trajectories crossing counts in each grid cell (resolution $0.2^\circ \cdot 0.2^\circ$).

53

54 3.7 Nucleation strength factor

55 The nucleation strength factor ($NSF_{15.7-100}$) is calculated as the ratio of fine to accumulation particle
 56 concentrations observed during nucleation day over the same ratio observed during non-event day (Salma
 57 et al., 2017). Fine and accumulation mode particle number concentrations ($N_{15.7-100}$ and $N_{100-800}$) were



retrieved from the SMPS data. The limited atmospheric residence time of fine particles (typically lower than 10h) means that a large portion of the $N_{15.7-100}$ concentration can also be related to local emissions and/or formation processes, including NPF events. On the contrary, due to a longer residence time within the atmosphere (up to 10 days), $N_{100-800}$ is more related to large spatial and temporal scales. Therefore, the numerator represents the increase of $N_{<100}$ relative to $N_{100-800}$ caused by all sources while the denominator represents the same property due to all sources except NPF. The NSF method is based on the hypothesis that aerosol sources are similar from day to day and from season to season, excepting the sporadic occurrence of NPF. Considering the large number of event (96) and non-event (432) days used to calculate $NSF_{15.7-100}$, one can assume that the sporadic/occasional (i.e. not observed on daily basis) sources of UF particles other than NPF events (e.g. volcanic plumes) have little impact on the $NSF_{15.7-100}$ in comparison to the sources always active (such as traffic, industries etc...).

NSF is generally used to better assess the contribution of NPF to fine particle number concentrations (represented by $N_{<100}$) relative to the regional background particle number concentrations. If the $NSF \approx 1$, then the relative contribution of NPF to particle number concentration with respect to other sources is negligible, like in Granada (Spain) urban site (Casquero-Vera et al., 2021). Moreover, Salma et al. (2017) also defined two thresholds for NSF_{6-100} to describe NPF contribution as a single source: a considerable contribution ($1 < NSF_{6-100} < 2$) or larger than of any other source sectors together ($NSF_{6-100} > 2$). One should keep in mind that these thresholds were defined accordingly to the lower cut off diameter originally set at 6nm. As the lower cut off diameter used in this study is a bit larger (15.7 nm instead of 6nm) than the one used by Salma et al. (2017), the calculated $NSF_{15.7-100}$ would necessarily be underestimated in comparison to NSF_{6-100} from Salma et al. (2017). The hourly median of fine to accumulation particle concentration ratio was computed for NPF event and non-event days. Figure 10 shows the $NSF_{15.7-100}$ diel variation observed at the ATOLL platform over 4 years of measurements. During spring, the $NSF_{15.7-100}$ factor remains quite constant (about 1.5) during night and morning and peaks at 16:00 UTC to reach a maximum at 2.5. This indicates that NPF has a significant effect on particle number concentration only a few (2-3) hours after the averaged NPF starting time. During summer, the tendency of the $NSF_{15.7-100}$ is quite similar with a unique peak at 13:00 UTC (again 2-3 hours after the



85 averaged NPF starting time). At that time the median $NSF_{15.7-100}$ values reach 4 while from 21:00 to 06:00
 86 UTC the $NSF_{15.7-100}$ remains low (averaged at 1.08). Therefore, during summer, the NPF contribution to
 87 particle number concentration is extremely high from 10:00 to 18:00 and then negligible for the rest of
 88 the day in comparison to other sources.
 89 Such NSF_{10-100} diel variations were observed in other European cities (Budapest, Vienna and Prague) with
 90 maximum reaching 2.7, 2.3 and 3.4 respectively with a lower cut-off diameter set at 10nm (Németh et al.,
 91 2018). Moreover, Salma et al. (2017) reported NSF_{6-100} peaks at midday varying from 2.2 and 2.7 for
 92 Budapest city center and from 2 to 7.2 for near city background for each season with NSF_{6-100} maximum
 93 reached during winter. The nucleation frequency during winter in Budapest is low ($<10\%$), similarly to
 94 our observations, however, the impact of these limited number of events on particle number
 95 concentrations is high. For the record, the $NSF_{15.7-100}$ factor peaked at 3.5 and 2.3 during winter and fall
 96 respectively.

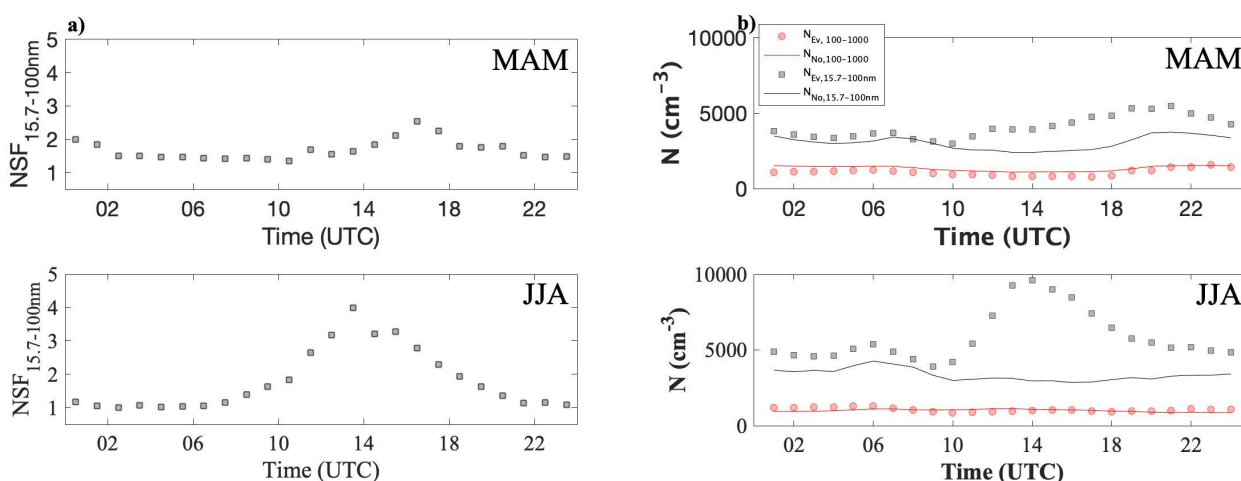


Figure 10 : (a) Diel variation of the Nucleation Strength Factor ($NSF_{15.7-100}$) during MAM and JJA calculated from number concentration during the 2017-2020 period. (b) Diel variation of particle number concentrations (N) for each season within the diameter ranges from 15.7 to 100 nm ($N_{15.7-100}$, black) and from 100 to 1000 nm ($N_{100-1000}$, red) at the ATOLL site during the 2017-2020 period. The dots correspond to event days while the line correspond to non-event days.



99 4 Conclusions

00 This study was based on 4-years (2017- 2020) measurements performed at the ATOLL site, in the close
01 vicinity of the city of Lille, Northern France. This paper is dedicated to studying new particle formation
02 (NPF) occurrence over a peri-urban site. The results highlight a strong seasonal variation of the NPF event
03 frequency, with a maximum occurrence observed during spring (23 %) and summer (26 %). The
04 undefined cases, which correspond to bursts of UFP that do not grow, are much more frequent (38% on
05 average) than NPF events all year long. The highest frequency (68%) is observed in August and the lowest
06 one (17%) in February. The interruption of the particle growth during undefined events can be mostly
07 attributed to changes of environmental conditions (irradiance and wind direction).

08 Seasonal variation of NPF parameters was also clearly observed and associated with environmental
09 parameters. High temperature ($T > 295\text{K}$), low RH ($\text{RH} < 45\%$) and high solar radiation favor the
10 occurrence of NPF events at ATOLL. The presence of clouds, linked to a decrease of solar radiation, is
11 limiting the NPF event occurrences. Moreover, NPF events start earlier in the morning during warmer
12 months (May-September) most probably related to variations in sunrise time. The growth rate calculated
13 between 15.7 and 30 nm ($\text{GR}_{15.7-30\text{nm}}$) ranges from 1.8 nm.h⁻¹ in March up to 10.9 nm.h⁻¹ in July. The
14 $\text{GR}_{15.7-30\text{nm}}$ was also found to be positively correlated with temperature. This correlation might be related
15 to larger emissions of biogenic precursors at higher temperatures, including monoterpenes known to favor
16 the occurrence of NPF event (Kulmala et al., 2004).

17 Relatively high values of Condensation Sink (averaged $\text{CS} > 2.10^{-2} \text{s}^{-1}$) are reported during NPF events
18 as well as during non-event days. These results suggest that high CS values are not limiting the NPF event
19 occurrence, consistent with recent studies focusing on NPF events over urban sites (Deng et al., 2020;
20 Hussein et al., 2020; Pushpawela et al., 2018). Looking more closely before the NPF onset (from 07:00 –
21 09:00 UTC), $\text{CS}_{07-09\text{h}}$ values are larger by 16% during non-event days. Interestingly, CS tends to increase
22 during event days (especially in summer) and size resolved CS clearly shows a peak shift from 150 nm
23 during non-event days to 50 nm during event days highlighting the strong contribution of newly formed
24 particles on CS.



25 Air masses trajectories (HYSPLIT) arriving over ATOLL during event days highlight a specific path
26 along the Eastern North Sea region with only a small fraction passing over any continental area and
27 therefore not crossing many anthropogenic sources, while, most of the back trajectories during non-event
28 days pass over large cities (Dunkirk, Paris, London, Rotterdam) before reaching Lille. The precursor
29 vapor concentration and probably their nature might differ from both “clean” and “polluted” air masses
30 and therefore promote or inhibit NPF event occurrences, a point which requires further investigation.

31

32 The impact of NPF events on particle number concentrations has been estimated through the nucleation
33 strength factor (NSF; Salma et al., 2017). The $NSF_{15.7-100nm}$ diel variation was calculated for spring and
34 summer occurring 2 to 3 hours after the average NPF starting time and reaching 1.5 and 4 during spring
35 and summer respectively. The extremely large $NSF_{15.7-100nm}$ value observed during summer highlights
36 the very high NPF contribution to the fine particles ($D_p < 100$ nm) number concentration in comparison
37 to other regional sources. Recently, (Ren et al., 2021) highlighted the strong impact of newly formed
38 particles from NPF on Cloud Condensation Nuclei (CCN) especially at sites close to anthropogenic
39 sources, such as ATOLL. In future studies, the impact of local vertical dynamics such as the effect of
40 boundary layer dynamics as in Lampilahti et al. (2020 and 2021) as well as the CCN enhancement factor
41 will be analysed.

42

43

44 **Acknowledgements**

45 This research was supported by the French national research agency (ANR) under the MABCaM (ANR-16-CE04-0009)
46 contract. Part of the instrumental system has been financially supported by the CaPPA project (Chemical and Physical
47 Properties of the Atmosphere), which is funded by the French National Research Agency (ANR) through the PIA (Programme
48 d'Investissement d'Avenir) under contract “ANR-11-LABX-0005-01”, and by the Regional Council “Hauts-de-France”. The
49 authors also thank the Région Hauts-de-France, and the Ministère de l'Enseignement Supérieur et de la Recherche (CPER
50 Climibio), and the European Fund for Regional Economic Development for their financial support. The authors gratefully
51 acknowledge the NOAA Air Resources Laboratory (ARL) for the provision of the HYSPLIT transport and dispersion model
52 and/or READY website (<https://www.ready.noaa.gov>) used in this publication. We thank Francois Thieuleux for ECMWF
53 data sharing during this work.



Data availability

ATOLL measurements are available through the EBAS database (<https://ebas.nilu.no>) and SMPS data before 2020 through <https://doi.org/10.5281/zenodo.6794562>. GDAS files for back-trajectory calculation are available at <https://www.arl.noaa.gov/hysplit/hysplit/>. NO_x data are available from the ATMO open data website : <https://data-atmo-hdf.opendata.arcgis.com>.

References :

- Barreira, L.M.F., Helin, A., Aurela, M., Teinilä, K., Friman, M., Kangas, L., Niemi, J.V., Portin, H., Kousa, A., Pirjola, L., Rönkkö, T., Saarikoski, S., Timonen, H., 2020. In-depth characterization of submicron particulate matter inter-annual variations at a street canyon site in Northern Europe (preprint). Aerosols/Field Measurements/Troposphere/Chemistry (chemical composition and reactions). <https://doi.org/10.5194/acp-2020-908>
- Berland, K., Rose, C., Pey, J., Culot, A., Freney, E., Kalivitis, N., Kouvarakis, G., Cerro, J.C., Mallet, M., Sartelet, K., Beckmann, M., Bourriane, T., Roberts, G., Marchand, N., Mihalopoulos, N., Sellegri, K., 2017. Spatial extent of new particle formation events over the Mediterranean Basin from multiple ground-based and airborne measurements. *Atmospheric Chem. Phys.* 17, 9567–9583. <https://doi.org/10.5194/acp-17-9567-2017>
- Bousiotis, D., Brean, J., Pope, F.D., Dall'Osto, M., Querol, X., Alastuey, A., Perez, N., Petäjä, T., Massling, A., Nøjgaard, J.K., Nordstrøm, C., Kouvarakis, G., Vratolis, S., Eleftheriadis, K., Niemi, J.V., Portin, H., Wiedensohler, A., Weinhold, K., Merkel, M., Tuch, T., Harrison, R.M., 2021. The effect of meteorological conditions and atmospheric composition in the occurrence and development of new particle formation (NPF) events in Europe. *Atmospheric Chem. Phys.* 21, 3345–3370. <https://doi.org/10.5194/acp-21-3345-2021>
- Bovchaliuk, V., Goloub, P., Podvin, T., Veselovskii, I., Tanre, D., Chaikovsky, A., Dubovik, O., Mortier, A.,



- 81 Lopatin, A., Korenskiy, M., Victori, S., 2016. Comparison of aerosol properties retrieved using GARRLiC, LIRIC,
 82 and Raman algorithms applied to multi-wavelength lidar and sun/sky-photometer data. *Atmos Meas Tech* 9, 3391–
 83 3405. <https://doi.org/10.5194/amt-9-3391-2016>
- 84 Boy, M., Kulmala, M., 2002. Influence of spectral solar irradiance on the formation of new particles in the
 85 continental boundary layer (preprint). <https://doi.org/10.5194/acpd-2-1317-2002>
- 86 Casquero-Vera, J.A., Lyamani, H., Titos, G., Minguillón, M.C., Dada, L., Alastuey, A., Querol, X., Petäjä, T.,
 87 Olmo, F.J., Alados-Arboledas, L., 2021. Quantifying traffic, biomass burning and secondary source contributions
 88 to atmospheric particle number concentrations at urban and suburban sites. *Sci. Total Environ.* 768, 145282.
 89 <https://doi.org/10.1016/j.scitotenv.2021.145282>
- 90 Chen, G., Canonaco, F., Tobler, A., Aas, W., Alastuey, A., Allan, J., Atabakhsh, S., Aurela, M., Baltensperger, U.,
 91 Bougiatioti, A., De Brito, J.F., Ceburnis, D., Chazeau, B., Chebaicheb, H., Daellenbach, K.R., Ehn, M., El Haddad,
 92 I., Eleftheriadis, K., Favez, O., Flentje, H., Font, A., Fossum, K., Freney, E., Gini, M., Green, D.C., Heikkinen, L.,
 93 Herrmann, H., Kalogridis, A.-C., Keernik, H., Lhotka, R., Lin, C., Lunder, C., Maasikmets, M., Manousakas, M.I.,
 94 Marchand, N., Marin, C., Marmureanu, L., Mihalopoulos, N., Močnik, G., Nęcki, J., O'Dowd, C., Ovadnevaite, J.,
 95 Peter, T., Petit, J.-E., Pikridas, M., Matthew Platt, S., Pokorná, P., Poulain, L., Priestman, M., Riffault, V., Rinaldi,
 96 M., Rózański, K., Schwarz, J., Sciare, J., Simon, L., Skiba, A., Slowik, J.G., Sosedova, Y., Stavroulas, I., Styszko,
 97 K., Teinmaa, E., Timonen, H., Tremper, A., Vasilescu, J., Via, M., Vodička, P., Wiedensohler, A., Zografou, O.,
 98 Cruz Minguillón, M., Prévôt, A.S.H., 2022. European Aerosol Phenomenology - 8: Harmonised Source
 99 Apportionment of Organic Aerosol using 22 Year-long ACSM/AMS Datasets. *Environ. Int.* 107325.
 00 <https://doi.org/10.1016/j.envint.2022.107325>
- 01 Clifford, S., Mazaheri, M., Salimi, F., Ezz, W.N., Yeganeh, B., Low-Choy, S., Walker, K., Mengersen, K., Marks,
 02 G.B., Morawska, L., 2018. Effects of exposure to ambient ultrafine particles on respiratory health and systemic
 03 inflammation in children. *Environ. Int.* 114, 167–180. <https://doi.org/10.1016/j.envint.2018.02.019>
- 04 Crumeyrolle S., Kontkanen J. SS, Rose C., Velasquez Garcia A., Bourrianne E., Catalfamo M., Riffault V., Tison
 05 E., Ferreira de Brito J., Visez N., Ferlay N., Auriol F., Chiapello I. : Measurement report: Atmospheric new particle
 06 formation in a peri-urban site in Lille, Northern France [Data set]. Zenodo.
 07 <https://doi.org/10.5281/zenodo.6794562>, 2022.
- 08 Cuesta-Mosquera, A., Močnik, G., Drinovec, L., Müller, T., Pfeifer, S., Minguillón, M., Björn, B., Buckley, P.,
 09 Dudoitis, V., Fernández-García, J., Fernández Amado, M., Brito, J., Flentje, H., Heffernan, E., Kalivitis, N.,
 10 Kalogridis, C., Keernik, H., Marmureanu, L., Luoma, K., Wiedensohler, A., 2020. Intercomparison and



- 11 characterization of 23 Aethalometers under laboratory and ambient air conditions: Procedures and unit-to-unit
- 12 variabilities. <https://doi.org/10.5194/amt-2020-344>
- 13 Dada, L., Paasonen, P., Nieminen, T., Buenrostro Mazon, S., Kontkanen, J., Peräkylä, O., Lehtipalo, K., Hussein,
- 14 T., Petäjä, T., Kerminen, V.-M., Bäck, J., Kulmala, M., 2017. Long-term analysis of clear-sky new particle
- 15 formation events and nonevents in Hyytiälä. *Atmospheric Chem. Phys.* 17, 6227–6241.
- 16 <https://doi.org/10.5194/acp-17-6227-2017>
- 17 Dal Maso, M., Kulmala, M., Riipinen, I., Wagner, R., Hussein, T., Aalto, P.P., Lehtinen, K.E.J., 2005. Formation
- 18 and growth of fresh atmospheric aerosols: Eight years of aerosol size distribution data from SMEAR II, Hyytiälä,
- 19 Finland. *Boreal Environ. Res.* 10, 323–336.
- 20 Dall’Osto, M., Beddows, D.C.S., Asmi, A., Poulain, L., Hao, L., Freney, E., Allan, J.D., Canagaratna, M., Crippa,
- 21 M., Bianchi, F., de Leeuw, G., Eriksson, A., Swietlicki, E., Hansson, H.C., Henzing, J.S., Granier, C., Zemankova,
- 22 K., Laj, P., Onasch, T., Prevot, A., Putaud, J.P., Sellegri, K., Vidal, M., Virtanen, A., Simo, R., Worsnop, D.,
- 23 O’Dowd, C., Kulmala, M., Harrison, R.M., 2018. Novel insights on new particle formation derived from a pan-
- 24 european observing system. *Sci. Rep.* 8, 1482. <https://doi.org/10.1038/s41598-017-17343-9>
- 25 Deng, C., Fu, Y., Dada, L., Yan, C., Cai, R., Yang, D., Zhou, Y., Yin, R., Lu, Y., Li, X., Qiao, X., Fan, X., Nie,
- 26 W., Kontkanen, J., Kangasluoma, J., Chu, B., Ding, A., Kerminen, V.-M., Paasonen, P., Worsnop, D.R., Bianchi,
- 27 F., Liu, Y., Zheng, J., Wang, L., Kulmala, M., Jiang, J., 2020. Seasonal Characteristics of New Particle Formation
- 28 and Growth in Urban Beijing. *Environ. Sci. Technol.* 54, 8547–8557. <https://doi.org/10.1021/acs.est.0c00808>
- 29 Dos Santos, V.N., Herrmann, E., Manninen, H.E., Hussein, T., Hakala, J., Nieminen, T., Aalto, P.P., Merkel, M.,
- 30 Wiedensohler, A., Kulmala, M., Petäjä, T., Hämeri, K., 2015. Variability of air ion concentrations in urban Paris.
- 31 *Atmospheric Chem. Phys.* 15, 13717–13737. <https://doi.org/10.5194/acp-15-13717-2015>
- 32 Duplissy, J., Merikanto, J., Franchin, A., Tsagkogeorgas, G., Kangasluoma, J., Wimmer, D., Vuollekoski, H.,
- 33 Schobesberger, S., Lehtipalo, K., Flagan, R.C., Brus, D., Donahue, N.M., Vehkamäki, H., Almeida, J., Amorim,
- 34 A., Barnet, P., Bianchi, F., Breitenlechner, M., Dunne, E.M., Guida, R., Henschel, H., Junninen, H., Kirkby, J.,
- 35 Kürten, A., Kupc, A., Määttänen, A., Makhmutov, V., Mathot, S., Nieminen, T., Onnela, A., Praplan, A.P.,
- 36 Riccobono, F., Rondo, L., Steiner, G., Tome, A., Walther, H., Baltensperger, U., Carslaw, K.S., Dommen, J.,
- 37 Hansel, A., Petäjä, T., Sipilä, M., Stratmann, F., Vrtala, A., Wagner, P.E., Worsnop, D.R., Curtius, J., Kulmala,
- 38 M., 2016. Effect of ions on sulfuric acid-water binary particle formation: 2. Experimental data and comparison with
- 39 QC-normalized classical nucleation theory: BINARY PARTICLE FORMATION EXPERIMENTS. *J. Geophys.*
- 40 *Res. Atmospheres* 121, 1752–1775. <https://doi.org/10.1002/2015JD023539>



- 41 Ganguly, D., Jayaraman, A., 2006. Physical and optical properties of aerosols over an urban location in western
 42 India: Implications for shortwave radiative forcing. *J. Geophys. Res. Atmospheres* 111.
 43 <https://doi.org/10.1029/2006JD007393>
- 44 Groß, J., Hamed, A., Sonntag, A., Spindler, G., Manninen, H.E., Nieminen, T., Kulmala, M., Hörrak, U., Plass-
 45 Dülmer, C., Wiedensohler, A., Birmili, W., 2018. Atmospheric new particle formation at the research station
 46 Melpitz, Germany: connection with gaseous precursors and meteorological parameters. *Atmospheric Chem. Phys.*
 47 18, 1835–1861. <https://doi.org/10.5194/acp-18-1835-2018>
- 48 Hamed, A., Korhonen, H., Sihto, S.-L., Joutsensaari, J., Järvinen, H., Petäjä, T., Arnold, F., Nieminen, T., Kulmala,
 49 M., Smith, J.N., Lehtinen, K.E.J., Laaksonen, A., 2011. The role of relative humidity in continental new particle
 50 formation. *J. Geophys. Res.* 116, D03202. <https://doi.org/10.1029/2010JD014186>
- 51 Jokinen, V., Mäkelä, J.M., 1997. Closed-loop arrangement with critical orifice for DMA sheath/excess flow system.
 52 *J. Aerosol Sci.* 28, 643–648. [https://doi.org/10.1016/S0021-8502\(96\)00457-0](https://doi.org/10.1016/S0021-8502(96)00457-0)
- 53 Kalkavouras, P., Bossioli, E., Bezantakos, S., Bougiatioti, A., Kalivitis, N., Stavroulas, I., Kouvarakis, G.,
 54 Protonotariou, A.P., Dandou, A., Biskos, G., Mihalopoulos, N., Nenes, A., Tombrou, M., 2017. New particle
 55 formation in the southern Aegean Sea during the Etesians: importance for CCN production and cloud droplet
 56 number. *Atmospheric Chem. Phys.* 17, 175–192. <https://doi.org/10.5194/acp-17-175-2017>
- 57 Kerminen, V.-M., Chen, X., Vakkari, V., Petäjä, T., Kulmala, M., Bianchi, F., 2018. Atmospheric new particle
 58 formation and growth: review of field observations. *Environ. Res. Lett.* 13, 103003. <https://doi.org/10.1088/1748-9326/aadf3c>
- 59 Kerminen, V.-M., Pirjola, L., Kulmala, M., 2001. How significantly does coagulational scavenging limit
 60 atmospheric particle production? *J. Geophys. Res. Atmospheres* 106, 24119–24125.
 61 <https://doi.org/10.1029/2001JD000322>
- 62 Kontkanen, J., Lehtipalo, K., Ahonen, L., Kangasluoma, J., Manninen, H.E., Hakala, J., Rose, C., Sellegri, K.,
 63 Xiao, S., Wang, L., Qi, X., Nie, W., Ding, A., Yu, H., Lee, S., Kerminen, V.-M., Petäjä, T., Kulmala, M., 2017.
 64 Measurements of sub-3 nm particles using a particle size magnifier in different environments: from clean mountain
 65 top to polluted megacities. *Atmospheric Chem. Phys.* 17, 2163–2187. <https://doi.org/10.5194/acp-17-2163-2017>
- 66 Kulmala, M., 2003. Atmospheric science. How particles nucleate and grow. *Science* 302, 1000–1001.
 67 <https://doi.org/10.1126/science.1090848>
- 68 Kulmala, M., Dal Maso, M., Mäkelä, J.M., Pirjola, L., Väkevä, M., Aalto, P., Mikkulainen, P., Hämeri, K.,
 69 O’Dowd, C.D., 2001. On the formation, growth and composition of nucleation mode particles. *Tellus Ser. B Chem.*
 70



- 71 Phys. Meteorol. 53, 479–490. <https://doi.org/10.1034/j.1600-0889.2001.530411.x>
- 72 Kulmala, M., Kerminen, V.-M., Petäjä, T., Ding, A.J., Wang, L., 2017. Atmospheric gas-to-particle conversion:
 73 why NPF events are observed in megacities? Faraday Discuss. 200, 271–288.
 74 <https://doi.org/10.1039/C6FD00257A>
- 75 Kulmala, M., Petäjä, T., Ehn, M., Thornton, J., Sipilä, M., Worsnop, D.R., Kerminen, V.-M., 2014. Chemistry of
 76 Atmospheric Nucleation: On the Recent Advances on Precursor Characterization and Atmospheric Cluster
 77 Composition in Connection with Atmospheric New Particle Formation. Annu. Rev. Phys. Chem. 65, 21–37.
 78 <https://doi.org/10.1146/annurev-physchem-040412-110014>
- 79 Kulmala, M., Petäjä, T., Nieminen, T., Sipilä, M., Manninen, H.E., Lehtipalo, K., Maso, M.D., Aalto, P.P.,
 80 Junninen, H., Paasonen, P., Riipinen, I., Lehtinen, K.E.J., Laaksonen, A., Kerminen, V.M., 2012. Measurement of
 81 the nucleation of atmospheric aerosol particles. Nat. Protoc. 7, 1651–1667. <https://doi.org/10.1038/nprot.2012.091>
- 82 Kulmala, M., Vehkamäki, H., Petäjä, T., Dal Maso, M., Lauri, A., Kerminen, V.-M., Birmili, W., McMurry, P.H.,
 83 2004. Formation and growth rates of ultrafine atmospheric particles: a review of observations. J. Aerosol Sci. 35,
 84 143–176. <https://doi.org/10.1016/j.jaerosci.2003.10.003>
- 85 Kurtén, T., Torpo, L., Ding, C.-G., Vehkamäki, H., Sundberg, M.R., Laasonen, K., Kulmala, M., 2007. A density
 86 functional study on water-sulfuric acid-ammonia clusters and implications for atmospheric cluster formation. J.
 87 Geophys. Res. Atmospheres 112. <https://doi.org/10.1029/2006JD007391>
- 88 Laj, P., Bigi, A., Rose, C., Andrews, E., Lund Myhre, C., Collaud Coen, M., Lin, Y., Wiedensohler, A., Schulz,
 89 M., Ogren, J.A., Fiebig, M., Gliß, J., Mortier, A., Pandolfi, M., Petäjä, T., Kim, S.-W., Aas, W., Putaud, J.-P.,
 90 Mayol-Bracero, O., Keywood, M., Labrador, L., Aalto, P., Ahlberg, E., Alados Arboledas, L., Alastuey, A.,
 91 Andrade, M., Artíñano, B., Ausmeel, S., Arsov, T., Asmi, E., Backman, J., Baltensperger, U., Bastian, S., Bath, O.,
 92 Beukes, J.P., Brem, B.T., Bukowiecki, N., Conil, S., Couret, C., Day, D., Dayantolis, W., Degorska, A.,
 93 Eleftheriadis, K., Fetfatzis, P., Favez, O., Flentje, H., Gini, M.I., Gregorič, A., Gysel-Beer, M., Hallar, A.G., Hand,
 94 J., Hoffer, A., Hueglin, C., Hooda, R.K., Hyvärinen, A., Kalapov, I., Kalivitis, N., Kasper-Giebl, A., Kim, J.E.,
 95 Kouvarakis, G., Kranjc, I., Krejci, R., Kulmala, M., Labuschagne, C., Lee, H.-J., Lihavainen, H., Lin, N.-H.,
 96 Löschau, G., Luoma, K., Marinoni, A., Martins Dos Santos, S., Meinhardt, F., Merkel, M., Metzger, J.-M.,
 97 Mihalopoulos, N., Nguyen, N.A., Ondracek, J., Pérez, N., Perrone, M.R., Petit, J.-E., Picard, D., Pichon, J.-M.,
 98 Pont, V., Prats, N., Prenni, A., Reisen, F., Romano, S., Sellegri, K., Sharma, S., Schauer, G., Sheridan, P., Sherman,
 99 J.P., Schütze, M., Schwerin, A., Sohmer, R., Sorribas, M., Steinbacher, M., Sun, J., Titos, G., Toczko, B., Tuch,
 00 T., Tulet, P., Tunved, P., Vakkari, V., Velarde, F., Velasquez, P., Villani, P., Vratolis, S., Wang, S.-H., Weinhold,



- 01 K., Weller, R., Yela, M., Yus-Diez, J., Zdimal, V., Zieger, P., Zikova, N., 2020. A global analysis of climate-
 02 relevant aerosol properties retrieved from the network of Global Atmosphere Watch (GAW) near-surface
 03 observatories. *Atmospheric Meas. Tech.* 13, 4353–4392. <https://doi.org/10.5194/amt-13-4353-2020>
- 04 Liao, L., Kerminen, V.-M., Boy, M., Kulmala, M., Dal Maso, M., 2014. Temperature influence on the natural
 05 aerosol budget over boreal forests. *Atmospheric Chem. Phys.* 14, 8295–8308. [https://doi.org/10.5194/acp-14-8295-](https://doi.org/10.5194/acp-14-8295-2014)
 06 2014
- 07 Lyubovtseva, Y.S., Sogacheva, L., Maso, M.D., Bonn, B., Keronen, P., Kulmala, M., 2005. Seasonal variations of
 08 trace gases, meteorological parameters, and formation of aerosols in boreal forests 10, 18.
- 09 Mazon, S.B., Riipinen, I., Schultz, D.M., Valtanen, M., Maso, M.D., Sogacheva, L., Junninen, H., Nieminen, T.,
 10 2009. Classifying previously undefined days from eleven years of aerosol-particle-size distribution data from the
 11 SMEAR II station, Hyytiälä, Finland. *Atmos Chem Phys* 10.
- 12 Merikanto, J., Duplissy, J., Määttä, A., Henschel, H., Donahue, N.M., Brus, D., Schobesberger, S., Kulmala,
 13 M., Vehkamäki, H., 2016. Effect of ions on sulfuric acid-water binary particle formation: 1. Theory for kinetic-
 14 and nucleation-type particle formation and atmospheric implications: BINARY PARTICLE FORMATION
 15 THEORY. *J. Geophys. Res. Atmospheres* 121, 1736–1751. <https://doi.org/10.1002/2015JD023538>
- 16 Mortier, A., Goloub, P., Podvin, T., Deroo, C., Chaikovsky, A., Ajtai, N., Blarel, L., Tanre, D., Derimian, Y., 2013.
 17 Detection and characterization of volcanic ash plumes over Lille during the Eyjafjallajökull eruption. *Atmos Chem*
 18 *Phys* 13, 3705–3720. <https://doi.org/10.5194/acp-13-3705-2013>
- 19 Németh, Z., Rosati, B., Zíková, N., Salma, I., Bozó, L., Dameto de España, C., Schwarz, J., Ždímal, V.,
 20 Wonaschütz, A., 2018. Comparison of atmospheric new particle formation events in three Central European cities.
 21 *Atmos. Environ.* 178, 191–197. <https://doi.org/10.1016/j.atmosenv.2018.01.035>
- 22 Nieminen, T., Kerminen, V.-M., Petäjä, T., Aalto, P.P., Arshinov, M., Asmi, E., Baltensperger, U., Beddows,
 23 D.C.S., Beukes, J.P., Collins, D., Ding, A., Harrison, R.M., Henzing, B., Hooda, R., Hu, M., Hörrak, U., Kivekäs,
 24 N., Komsaare, K., Krejci, R., Kristensson, A., Laakso, L., Laaksonen, A., Leaitch, W.R., Lihavainen, H.,
 25 Mihalopoulos, N., Németh, Z., Nie, W., O'Dowd, C., Salma, I., Sellegri, K., Svenningsson, B., Swietlicki, E.,
 26 Tunved, P., Ulevicius, V., Vakkari, V., Vana, M., Wiedensohler, A., Wu, Z., Virtanen, A., Kulmala, M., 2018.
 27 Global analysis of continental boundary layer new particle formation based on long-term measurements.
 28 *Atmospheric Chem. Phys.* 18, 14737–14756. <https://doi.org/10.5194/acp-18-14737-2018>
- 29 Ohlwein, S., Kappeler, R., Kutlar Joss, M., Künzli, N., Hoffmann, B., 2019. Health effects of ultrafine particles: a
 30 systematic literature review update of epidemiological evidence. *Int. J. Public Health* 64, 547–559.



- 31 <https://doi.org/10.1007/s00038-019-01202-7>
- 32 Paasonen, P., Peltola, M., Kontkanen, J., Junninen, H., Kerminen, V.-M., Kulmala, M., 2018. Comprehensive
33 analysis of particle growth rates from nucleation mode to cloud condensation nuclei in boreal forest. *Atmospheric*
34 *Chem. Phys.* 18, 12085–12103. <https://doi.org/10.5194/acp-18-12085-2018>
- 35 Peng, Y., Dong, Y., Li, X., Liu, X., Dai, J., Chen, C., Dong, Z., Du, C., Wang, Z., 2017. Different Characteristics
36 of New Particle Formation Events at Two Suburban Sites in Northern China. *Atmosphere* 8, 258.
37 <https://doi.org/10.3390/atmos8120258>
- 38 Pierce, J.R., Adams, P.J., 2009. Uncertainty in global CCN concentrations from uncertain aerosol nucleation and
39 primary emission rates. *Atmospheric Chem. Phys.* 9, 1339–1356. <https://doi.org/10.5194/acp-9-1339-2009>
- 40 Ren, J., Chen, L., Fan, T., Liu, J., Jiang, S., Zhang, F., 2021. The NPF Effect on CCN Number Concentrations: A
41 Review and Re-Evaluation of Observations From 35 Sites Worldwide. *Geophys. Res. Lett.* 48, e2021GL095190.
42 <https://doi.org/10.1029/2021GL095190>
- 43 Rodríguez, S., Cuevas, E., González, Y., Ramos, R., Romero, P.M., Pérez, N., Querol, X., Alastuey, A., 2008.
44 Influence of sea breeze circulation and road traffic emissions on the relationship between particle number, black
45 carbon, PM₁, PM_{2.5} and PM_{2.5–10} concentrations in a coastal city. *Atmos. Environ.* 42, 6523–6534.
46 <https://doi.org/10.1016/j.atmosenv.2008.04.022>
- 47 Rodríguez, S., Van Dingenen, R., Putaud, J.-P., Martins-Dos Santos, S., Roselli, D., 2005. Nucleation and growth
48 of new particles in the rural atmosphere of Northern Italy—relationship to air quality monitoring. *Atmos. Environ.*
49 39, 6734–6746. <https://doi.org/10.1016/j.atmosenv.2005.07.036>
- 50 Roig Rodelas, R., Chakraborty, A., Perdrix, E., Tison, E., Riffault, V., 2019. Real-time assessment of wintertime
51 organic aerosol characteristics and sources at a suburban site in northern France. *Atmos. Environ.* 203, 48–61.
52 <https://doi.org/10.1016/j.atmosenv.2019.01.035>
- 53 Rolph, G., Stein, A., Stunder, B., 2017. Real-time Environmental Applications and Display sYstem: READY.
54 *Environ. Model. Softw.* 95, 210–228. <https://doi.org/10.1016/j.envsoft.2017.06.025>
- 55 Rose, C., Sellegri, K., Asmi, E., Hervo, M., Freney, E., Colomb, A., Junninen, H., Duplissy, J., Sipilä, M.,
56 Kontkanen, J., Lehtipalo, K., Kulmala, M., 2015a. Major contribution of neutral clusters to new particle formation
57 at the interface between the boundary layer and the free troposphere. *Atmospheric Chem. Phys.* 15, 3413–3428.
58 <https://doi.org/10.5194/acp-15-3413-2015>
- 59 Rose, C., Sellegri, K., Freney, E., Dupuy, R., Colomb, A., Pichon, J.-M., Ribeiro, M., Bourianne, T., Burnet, F.,
60 Schwarzenboeck, A., 2015b. Airborne measurements of new particle formation in the free troposphere above the



- 61 Mediterranean Sea during the HYMEX campaign. *Atmospheric Chem. Phys.* 15, 10203–10218.
 62 <https://doi.org/10.5194/acp-15-10203-2015>
- 63 Rose, C., Sellegri, K., Moreno, I., Velarde, F., Ramonet, M., Weinhold, K., Krejci, R., Andrade, M., Wiedensohler,
 64 A., Ginot, P., Laj, P., 2017. CCN production by new particle formation in the free troposphere. *Atmospheric Chem.*
 65 *Phys.* 17, 1529–1541. <https://doi.org/10.5194/acp-17-1529-2017>
- 66 Salimi, F., Rahman, M.M., Clifford, S., Ristovski, Z., Morawska, L., 2017. Nocturnal new particle formation events
 67 in urban environments. *Atmospheric Chem. Phys.* 17, 521–530. <https://doi.org/10.5194/acp-17-521-2017>
- 68 Salma, I., Németh, Z., Kerminen, V.-M., Aalto, P., Nieminen, T., Weidinger, T., Molnár, Á., Imre, K., Kulmala,
 69 M., 2016. Regional effect on urban atmospheric nucleation. *Atmospheric Chem. Phys.* 16, 8715–8728.
 70 <https://doi.org/10.5194/acp-16-8715-2016>
- 71 Sandradewi, J., Prévôt, A.S.H., Szidat, S., Perron, N., Alfarra, M.R., Lanz, V.A., Weingartner, E., Baltensperger,
 72 U., 2008. Using aerosol light absorption measurements for the quantitative determination of wood burning and
 73 traffic emission contributions to particulate matter. *Environ. Sci. Technol.* 42, 3316–3323.
- 74 Sellegri, K., Rose, C., Marinoni, A., Lupi, A., Wiedensohler, A., Andrade, M., Bonasoni, P., Laj, P., 2019. New
 75 Particle Formation: A Review of Ground-Based Observations at Mountain Research Stations. *Atmosphere* 10, 493.
 76 <https://doi.org/10.3390/atmos10090493>
- 77 Shukla, K.K., Niranjana Kumar, K., Phanikumar, D.V., Newsom, R.K., Kotamarthi, V.R., Ouarda, T.B.M.J.,
 78 Ratnam, M.V., 2016. Identification of the cloud base height over the central Himalayan region: Intercomparison of
 79 Ceilometer and Doppler Lidar (preprint). *Clouds/Remote Sensing/Validation and Intercomparisons*.
 80 <https://doi.org/10.5194/amt-2016-162>
- 81 Sogacheva, L., Hamed, A., Facchini, M.C., Kulmala, M., Laaksonen, A., 2007. Relation of air mass history to
 82 nucleation events in Po Valley, Italy, using back trajectories analysis. *Atmos Chem Phys* 15.
- 83 Sogacheva, L., Maso, M.D., Kerminen, V.M., Kulmala, M., 2005. Probability of nucleation events and aerosol
 84 particle concentration in different air mass types arriving at Hyytiälä southern Finland, based on back trajectories
 85 analysis. *Boreal Environ. Res.* 10, 479–491.
- 86 Spracklen, D.V., Carslaw, K.S., Kulmala, M., Kerminen, V.-M., Mann, G.W., Sihto, S.-L., 2006. The contribution
 87 of boundary layer nucleation events to total particle concentrations on regional and global scales. *Atmospheric*
 88 *Chem. Phys.* 6, 5631–5648. <https://doi.org/10.5194/acp-6-5631-2006>
- 89 Stein, A.F., Draxler, R.R., Rolph, G.D., Stunder, B.J.B., Cohen, M.D., Ngan, F., 2015. NOAA's HYSPLIT
 90 Atmospheric Transport and Dispersion Modeling System. *Bull. Am. Meteorol. Soc.* 96, 2059–2077.



- 91 <https://doi.org/10.1175/BAMS-D-14-00110.1>
- 92 Tuch, T.M., Herbarth, O., Franck, U., Peters, A., Wehner, B., Wiedensohler, A., Heintzenberg, J., 2006. Weak
93 correlation of ultrafine aerosol particle concentrations <800 nm between two sites within one city. *J. Expo. Sci.*
94 *Environ. Epidemiol.* 16, 486–490. <https://doi.org/10.1038/sj.jes.7500469>
- 95 Tunved, P., Hansson, H.-C., Kerminen, V.-M., Ström, J., Dal Maso, M., Lihavainen, H., Viisanen, Y., Aalto, P.P.,
96 Komppula, M., Kulmala, M., 2006. High natural aerosol loading over boreal forests. *Science* 312, 261–263.
97 <https://doi.org/10.1126/science.1123052>
- 98 Villani, P., Picard, D., Marchand, N., Laj, P., 2007. Design and validation of a 6-volatility tandem differential
99 mobility analyzer (VTDMA). *Aerosol Sci. Technol.* 41, 898–906. <https://doi.org/10.1080/02786820701534593>
- 00 Wang, Z., Wu, Z., Yue, D., Shang, D., Guo, S., Sun, J., Ding, A., Wang, L., Jiang, J., Guo, H., Gao, J., Cheung,
01 H.C., Morawska, L., Keywood, M., Hu, M., 2017. New particle formation in China: Current knowledge and further
02 directions. *Sci. Total Environ.* 577, 258–266. <https://doi.org/10.1016/j.scitotenv.2016.10.177>
- 03 Wang, Z.B., Hu, M., Wu, Z.J., Yue, D.L., Zheng, J., Zhang, R.Y., Pei, X.Y., Paasonen, P., Dal Maso, M., Boy, M.,
04 Wiedensohler, A., 2013. Investigation of the connections between atmospheric new particle formation and organics
05 at an urban site of Beijing (preprint). *Aerosols/Field Measurements/Troposphere/Chemistry (chemical composition*
06 *and reactions)*. <https://doi.org/10.5194/acpd-13-3419-2013>
- 07 Wehner, B., Wiedensohler, A., 2003. Long term measurements of submicrometer urban aerosols: statistical
08 analysis for correlations with meteorological conditions and trace gases. *Atmospheric Chem. Phys.* 3, 867–879.
09 <https://doi.org/10.5194/acp-3-867-2003>
- 10 Xiao, S., Wang, M.Y., Yao, L., Kulmala, M., Zhou, B., Yang, X., Chen, J.M., Wang, D.F., Fu, Q.Y., Worsnop,
11 D.R., Wang, L., 2015. Strong atmospheric new particle formation in winter in urban Shanghai, China. *Atmospheric*
12 *Chem. Phys.* 15, 1769–1781. <https://doi.org/10.5194/acp-15-1769-2015>
- 13 Yao, L., Garmash, O., Bianchi, F., Zheng, J., Yan, C., Kontkanen, J., Junninen, H., Mazon, S.B., Ehn, M., Paasonen,
14 P., Sipilä, M., Wang, M., Wang, X., Xiao, S., Chen, H., Lu, Y., Zhang, B., Wang, D., Fu, Q., Geng, F., Li, L.,
15 Wang, H., Qiao, L., Yang, X., Chen, J., Kerminen, V.-M., Petäjä, T., Worsnop, D.R., Kulmala, M., Wang, L., 2018.
16 Atmospheric new particle formation from sulfuric acid and amines in a Chinese megacity. *Science* 361, 278–281.
17 <https://doi.org/10.1126/science.aao4839>
- 18 Yli-Juuti, T., Nieminen, T., Hirsikko, A., Aalto, P.P., Asmi, E., Hörrak, U., Manninen, H.E., Patokoski, J., Dal
19 Maso, M., Petäjä, T., Rinne, J., Kulmala, M., Riipinen, I., 2011. Growth rates of nucleation mode particles in
20 Hyytiälä during 2003–2009: variation with particle size, season, data analysis method and ambient conditions.



21 Atmospheric Chem. Phys. 11, 12865–12886. <https://doi.org/10.5194/acp-11-12865-2011>

22

23